ARTICLE **OPEN**

Check for updates

Flexible radio-frequency micro electro-mechanical switch towards the applications of satellite communications

Yingli Shi[1,2], Chao Zhou[2], Zibo Cao[2], Yurong He[2], Jingwen Guo[2], Chunxin Li[2], Qianhong Wu[2], Kui Liang [2✉], Yanzhao Li[2✉] and Yuan Lin [1✉]

This paper presents a flexible radio-frequency microelectromechanical system (RF MEMS) switch integrated on cyclo-olefin polymer (COP) substrate using a modified surface MEMS processing technology, which could be used in the 17–19 GHz frequency band of satellite communication. Through systematic simulation analysis, it is found that flexible RF MEMS switch can achieve certain bending radius by miniaturizing the electronic dimension, without degrading the RF performance. It is demonstrated that the RF characteristics of flexible RF MEMS switch with special anchor structural design, fabricated by modified surface MEMS processing, are not sensitive to bending deformation under the curvature of 0 mm^{-1}, 0.05 mm^{-1}, 0.10 mm^{-1}. Furthermore, the range of bending curvature which will affect the RF characteristics is given through systematic simulation. The flexible RF MEMS switch with high process compatibility and stable RF performance is believed to be promising candidates for future microwave communications and other consumer electronics.

INTRODUCTION

The evolution of technology has brought us the era of flexible electronics, which is far beyond the scope of the application fields for conventional rigid electronics[1,2]. Flexible electronics trigger plenty of interest in applications, such as portable display[3,4], wearable health care[5,6], flexible communication[7–10], flexible sensors[11–13], flexible energy conversion[14,15] and so on, for the merit of the advantages in weight, volume, and portability. The wireless data transmission of flexible electronics has provoked great research interest in the last few years. One of the widely used strategies is to integrate rigid data transmission chips and other devices through flexible substrate[16] or flexible structures[17]. However, this solution will debase the flexibility of the system to a great extent. In order to settle this problem, flexible RF devices for communication have been demonstrated recently, such as flexible film bulk acoustic wave resonators (FBARs)[18,19], antennas[20,21], transmission lines[22,23], supercapacitors[24], and high cut-off transistors[25–27]. The flexible devices based on the mechano-electrical coupling strategy[12,28–31] provide feasible solutions to the requirements of flexible conformal or stretchable RF applications[32–34].

RF MEMS refer to electronics manufactured by MEMS processing technology to replace traditional devices in the field of radio frequency (RF) and microwave, and improve various functional parameters of traditional RF and microwave devices with the help of many advantages of MEMS, for example, lower power consumption and isolation loss, and higher cut-off frequency. Therefore, it has broader application prospects in many fields such as switches, capacitors, filters, phase shifters, amplifiers, reconfigurable antenna and so on[35]. Flexible RF MEMS[36,37] play an irreplaceable role in flexible communications for reliable microwave performance and ultralow-power consumption. With the advantages of conformal, flexible, impact resistant, and low cost, flexible RF MEMS are very suitable for airborne/space borne radar or internet of things communication system.

In satellite systems, the cost of launching a satellite is hundreds of thousands of dollars per kilogram of payload. The communication subsystem accounts for more than 15% of the satellite load. Flexible reconfigurable RF MEMS can not only ensure lightweight, high integration and high performance, but also meet the requirements of large curvature bending or stretchable conformal integration in satellite communication applications, which includes flexible RF MEMS switch matrix[38,39], MEMS phase shifters[40,41], reconfigurable MEMS antennas and phased array MEMS antennas[42,43]. As the basic structural unit of the above applications, it can be integrated with the large curvature or stretchable flexible RF MEMS system through ingenious mechanical structure design, such as island-bridge[44] or fractal[45] structure design connecting the MEMS units. In this way, the single MEMS unit in the system, serving as the island in the island-bridge structure or the node in the fractal connection, only need to stand a certain degree of curvature. The pioneers have carried out research on RF MEMS from different aspects such as structure, material, preparation process and theoretical modeling, such as, double-clamped beam switch based on flexible liquid crystal polymer (LCP) substrate[46], RF MEMS switch fabricated on a flexible organic substrate (FR-4) by the wafer transfer technology (WTT)[47], thin film silicon beam micro-resonator on flexible polyethylene terephthalate substrates with a low processing temperature[48], double-clamped beam resonator based on a ultrathin (10 μm thick) flexible polyimide substrate[49].

Existing studies indicate that the performance of flexible RF MEMS devices are significantly affected by bending deformation, both driving characteristics and RF characteristics[50–53], as shown in Table 1. Especially, research on the multi-physical field models of flexible RF MEMS switch under bending deformation shows that when the bending curvature of the substrate increases from 0 m^{-1} to 28.6 m^{-1}, the return loss S_{11} of the On state flexible RF MEMS switch deteriorates from -27.1 dB to -22.0 dB, with a decreasing rate up to 18.9%[52].

[1]School of Materials and Energy, University of Electronic Science and Technology of China (USETC), Chengdu, China. [2]BOE Technology Innovation Center, BOE Technology Group Co Ltd, Beijing, China. ✉email: liangkui@boe.com.cn; liyanzhao@boe.com.cn; linyuan@uestc.edu.cn

Table 1. Comparison of the performance of Flexible RF MEMS under bending condition.

Type of flexible RF MEMS	Bending radius	Return loss (S_{11}) flat/curved substrate	Actuation principle	Reference
Double Clamped Beam MEMS Switch	22.6 mm	−18 dB @ 20 GHz/Null	Electro-static	[50]
V-Shaped Beam MEMS Switch	30.0 mm	RF Characteristics Null, Actuation Current Changes 13.70%	Electro-thermal	[51]
Double Clamped Beam MEMS Switch	35.0 mm	−27.1 dB/−22.0 dB @ 10 GHz	Electro-static	[52]
Low-pass RF MEMS Filter	35.0 mm	−22.7 dB/−5.7 dB @ 10 GHz	Null	[53]

However, the flexible RF MEMS with stable RF performance under curved condition has not yet been demonstrated, mainly due to the difficulty of compatibility between the fabrication process of miniaturized MEMS and high performance. In the published results, the length of the flexible RF MEMS switch membrane beam with a double-clamped beam structure is basically about 500 µm or even longer, the thickness of the membrane beam is about 1 or 2 µm. The driving voltage of the RF MEMS switch of this size is generally in the order of tens of volts, which is more in line with the voltage range of commonly used communication equipment. For example, Zhang's team proposed two sizes of FR-4 substrate-based flexible RF MEMS switch membrane beams with lengths of 400 µm[48] and 800 µm[54], thicknesses of 1 µm, and drive voltages of about 25 V to 35 V. Han's team proposed an LCP substrate-based flexible RF MEMS switch membrane beam with a length of 600 µm[50,52], a thickness of 2 µm, and a drive voltage of about 50 V. However, when the beam span is reduced to 120 µm, the driving voltage required for the beam with a thickness of 2 µm will be up to 550 V. Confronting this problem, it is believed that reducing the thickness of the MEMS membrane beam is a very effective and easy-to-think solution to maintain a low driving voltage while miniaturizing the MEMS membrane beam structure. For instance, a 0.2-µm-thick beam with the length of 120 µm corresponds to 80 V driving voltage, as shown in Supplementary Fig. 1.

In this work, we developed and fabricated a flexible RF MEMS switch with stable performance under curved condition and high process compatibility, which is designed within the frequency band of 17–19 GHz for satellite communication applications, corresponding to Ku/K band[55]. Modified surface MEMS processing technology based on flexible cyclo-olefin polymers (COP) thin film substrate[56] is adopted to fabricate flexible RF MEMS switch. Special anchor structure with three-side support cavity structure has been designed in order to avoid the adhesion or peeling of MEMS membrane beam. The reflection loss (S_{11}) of the flexible RF MEMS switch at on state exceeds -18 dB in the frequency band of 17–19 GHz with a driving voltage of 60 V. Two bending radii of 10 mm and 20 mm are achieved without degrading performance. Furthermore, the range of bending curvature which will affect the RF characteristics is given through systematic simulation. As the basic structural unit, a flexible RF MEMS switch determines the performance of flexible reconfigurable RF devices based on MEMS switch in the bending conformal integration scenario. The realization of flexible RF MEMS switch with high process compatibility and stable RF performance will promote a key step for the development of flexible reconfigurable devices (MEMS phase shifters, reconfigurable antennas and phased array antennas etc.) based on MEMS and other applications of Flexible MEMS (sensor and actuator etc.) with movable components.

RESULTS

Miniaturized flexible RF MEMS switch for large curvature

The flexible double-clamped beam RF MEMS switch structure is shown in Fig. 1a. The MEMS membrane beam is suspended on the signal line of the coplanar waveguide (CPW), and a dielectric layer is laid on the signal line. The driving voltage is applied between the signal line and the membrane beam to supply a pull-down electrostatic driving force for the beam. When the beam is pulled down by electrostatic force to be attached to the signal line, the switch will turn to the closed state, as shown in Fig. 1b i and b ii. When the flexible RF MEMS switch under large curvature bending condition, the gap between the suspending beam and the signal will various greatly, which will lead to great impact in the driving characteristics and RF characteristics of the switch, as shown in Fig. 1b iii and b iv. By miniaturizing the electronic dimension, the flexible RF MEMS can achieve certain bending radius without degrading the performance. Special anchor structure and modified surface MEMS processing technology are introduced to design and fabricate the miniaturized flexible RF MEMS switch with stable performance and high process compatibility. The miniaturized design flexible RF MEMS switch attached to a curved frame with a curvature radius of 10 mm is shown in Fig. 1c. The dimensions of the RF MEMS switch are as follows: beam length 120 µm, beam width 20 µm, beam thickness 0.2 µm, the suspending beam gap 2 µm, the signal width 40 µm, the distance between the central signal line and ground is 40 µm, and the thickness of the CPW is 1 µm, shown in Fig. 1d.

Finite element analysis (FEA) is performed to evaluate the mechanical and RF characteristics of the flexible RF MEMS switch, through the multi-physical field simulation method based on ANSYS Workbench. The driving characteristics and RF characteristics of the switch in the on and off states with bending curvature of 0 mm^{-1} (flat substrate), 0.05 mm^{-1} and 0.1 mm^{-1} are simulated. The electrostatic drive and RF characteristics are simulated through Maxwell 3D, Static Structure, and HFSS modules in ANSYS Workbench. See the FEM multi-physics field analysis section and Supplementary Fig. 2 for the simulation process details.

The reflection loss S_{11} and insertion loss S_{21} characteristics of the flexible RF MEMS switch under variety of bending conditions calculated from the simulation show high consistency as shown in Fig. 1e–h. S_{11} of on state RF MEMS switch with different curvature remains at about -27 dB in the frequency band of 15–20 GHz, and the value various range within 1 dB. In sharp contrast, the variation range in the previous results reached more than 5 dB[52]. S_{21} of on state RF MEMS switch with different curvature maintains within the range of -0.03 dB to -0.06 dB. It can be seen from the FEA model that under the bending deformation of the flexible RF MEMS switch with curvature of 0.05 mm^{-1} and 0.1 mm^{-1}, the suspending beam gap hardly changes, and the parallel capacitance of on state does not change significantly, which leads to almost negligible impact on the RF characteristics. S_{11} and S_{21} of off state RF MEMS switch with different curvature maintain within the range of -0.07 dB to - 0.09 dB. S_{11} and S_{21} of the off state under different bending curvature are less different than those of the on state, which are almost consistent at the corresponding frequencies. For the S_{11} and S_{21} of off state, the electrostatic driven membrane beam is in contact with the signal line. Bending deformation will not transform the attachment state, which means no matter how large the bending curvature is, it will not have a significant impact on these two RF parameters.
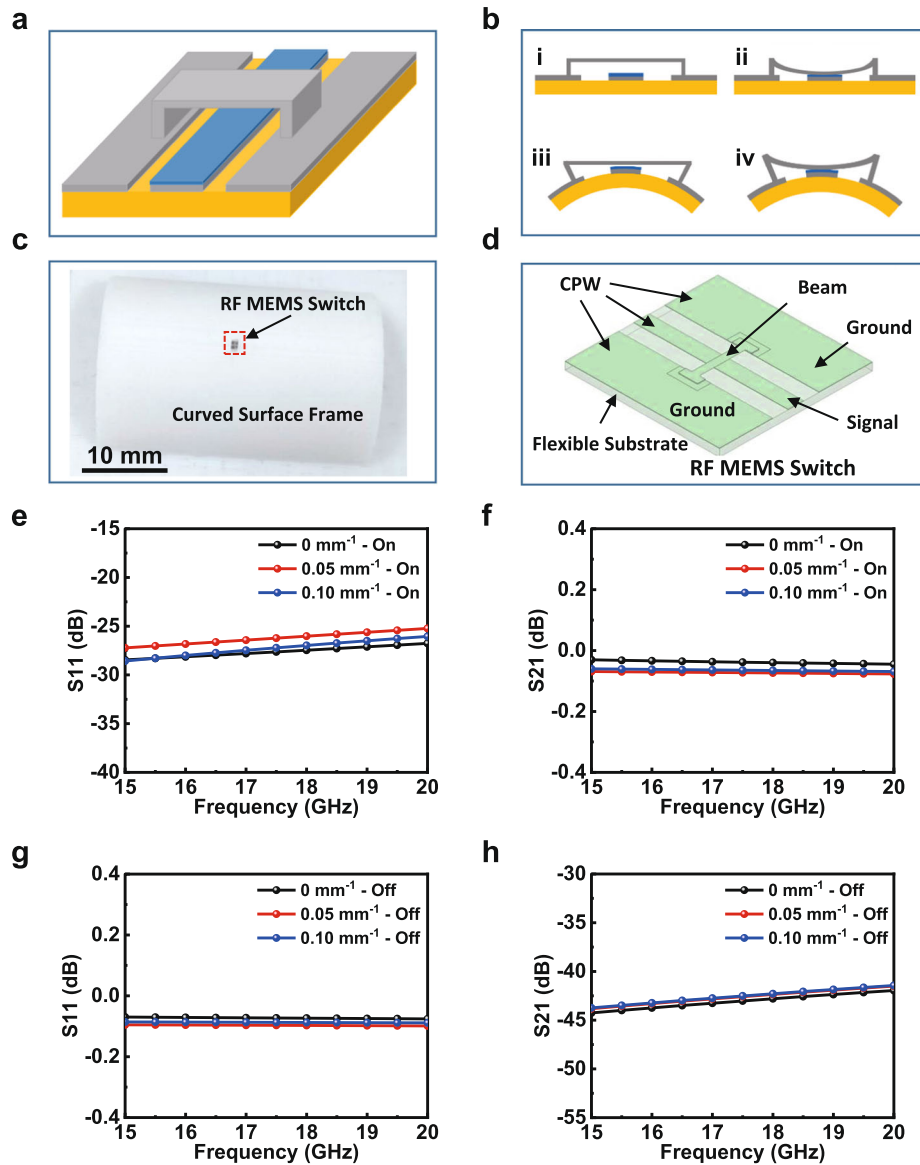
Fig. 1 **Miniaturized flexible RF MEMS switch for large curvature. a** Schematic diagram of flexible double-clamped beam RF MEMS switch. **b** Configuration diagram of flexible RF MEMS switch in different modes: i) On state and ii) Off state of MEMS switch with flat substrate; iii) On state and iv) Off state of MEMS switch with curved substrate. **c** Image of a miniaturized MEMS switch attached to a curved surface. **d** Structure of miniaturized MEMS switch. **e** On state S_{11}, (**f**) On state S_{21}, (**g**) Off state S_{11} and **h** Off state S_{21} of membrane beam under different bending curvatures.

Flexible RF MEMS switch design and fabrication for characterization

To demonstrate the RF performance of the proposed RF MEMS switch under the flexible deformation of the substrate, the flexible RF MEMS switch is fabricated based on special anchor design and modified surface MEMS process technology. The RF MEMS switch unit with characteristic impedance of 100 Ω is connected with the CPW test port with characteristic impedance of 50 Ω through the impedance transformation of 1/4 design frequency (17.7 GHz) wavelength, so that the RF performance can be measured by feeding the SubMiniature version A (SMA) connector, as shown in Fig. 2a and Supplementary Fig. 3a. A customized SMA connector with an impedance of 50 Ω (frequency: DC - 40 GHz) is designed as shown in Fig. 5 and Supplementary Fig. 8 for the RF performance measurement. Figure 2a shows the overall design of the proposed flexible RF MEMS switch. The partial enlarged view of the RF MEMS switch unit is shown in Fig. 2b, in which the red dumbbell structure demonstrates the membrane beam of the MEMS switch. Here, the MEMS switch adopts the electrostatic drive strategy to achieve the On state and Off state of the switch by controlling the DC bias voltage, as shown in Supplementary Fig. 3c. In order to avoid the crosstalk between DC driving signal and RF signal during the measurement and eliminate the breakdown risk of DC voltage to the measurement equipment during the measurement, the structural design of separating the applied DC drive voltage from RF signal is adopted to realize the controllability and reliability of the structure and the safety of the measurement equipment, as shown in Fig. 2b, d. The anchors at both ends of the beam adopt the cavity structural design of three-side support to ensure that the suspending thin beam can be fabricated successfully, as shown in Fig. 2c. The equivalent-circuit model of the RF MEMS switch is shown in Supplementary Fig. 3b. Z_L is the characteristic impedance of the CPW transmission line under the membrane beam, $Z_{1/4\lambda}$ is the resistance of the 1/4λ impedance transformation line, Z_0 is the characteristic impedance of the test port CPW, C is
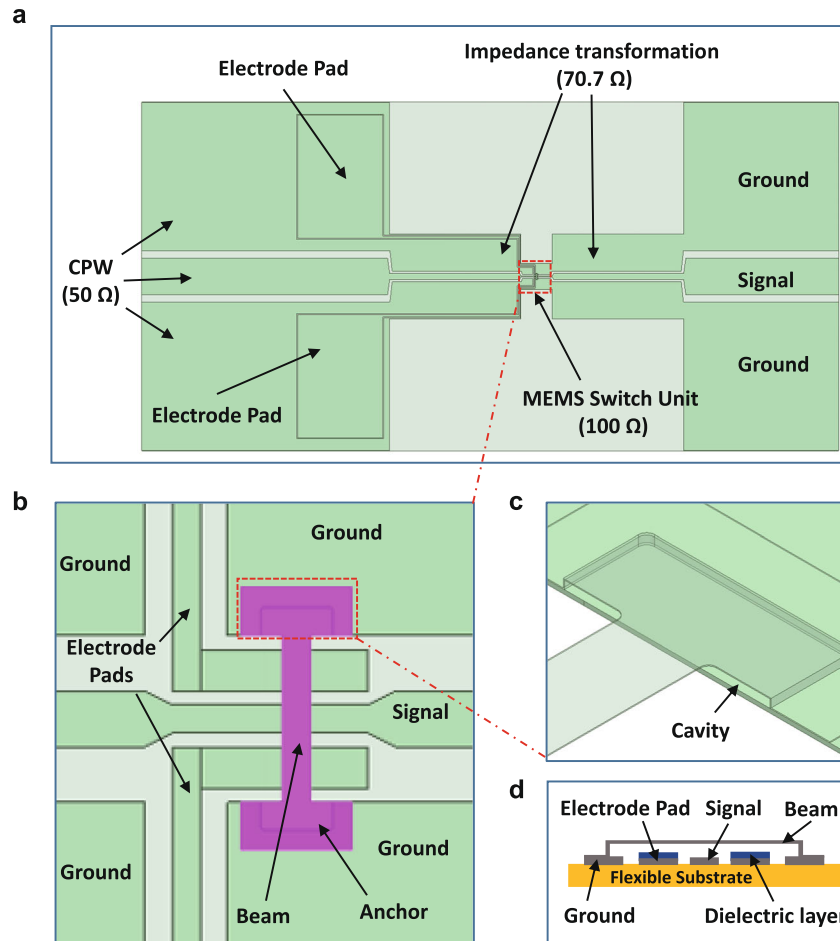
Fig. 2 Flexible RF MEMS switch design for characterization. a Design of RF MEMS switch including test port and impedance transformation. **b** Partial enlarged view of RF MEMS switch unit design. **c** Anchor structural design of three-side support cavity. **d** Side view of schematic diagram of RF MEMS switch.

the parallel capacitance generated between the membrane beam and the signal line, R is the resistance of the membrane beam of the electrostatic driving electrodes, and L is the inductance of the membrane beam of the driving electrodes.

Based on the flexible RF MEMS design, the mask layout of the surface MEMS process, the structural design details, and dimensions of the flexible RF MEMS switch indicated on the mask are shown in Supplementary Fig. 4. For fabrication of the switch, modified surface MEMS process flow is carried out. The preparation and release of the sacrificial layer is the critical process in the fabrication of the device. The photoresist with natural flow flattening is used as the sacrificial layer, and the wet release method is utilized to release the sacrificial layer. The process parameters need to be strictly controlled. To fabricate the suspending thin membrane beam, magnetron sputtering deposition is utilized to take over the common electroplating process for MEMS beam fabrication, considering that the thickness of the beam designed is only 0.2 μm. In order to solve the curling or bulking of the membrane beam, the residual stress of the beam metal layer structure is reduced by segmented multiple deposition. More details of the surface MEMS process flow are described in the Methods section.

It is worth noting that the flexible COP film used in this work has been widely used as substrate for flexible consumer electronics (e.g. flexible antenna on screen), due to its ultra-high optical transmittance, RF characteristics of low losses[56]. Our flexible MEMS device based on COP substrate and high process compatibility has great potential to integrate with other flexible or highly integrated

electronic components (e.g. RF front-end, interconnections, LEDs) to form a multifunctional flexible consumer electronics system.

Figure 3a demonstrates the optical microscope morphology of the fabricated flexible RF MEMS switch, showing the top and oblique view of the intact and clean switch structure. Figure 3b shows the surface morphology of the RF MEMS switch measured by the 3D surface morphology instrument. The thickness of the switch and the height of the cavity layer can be finally measured through the scanning results. The flexible RF MEMS switch with COP substrate can be attached to the surface of objects in various shapes. In Fig. 3c, the flexible RF MEMS switch is adhered to a 3D printed curved surface frame with a radius of 10 mm conformally. 3D surface topography contour of flexible RF MEMS switch in membrane beam driving state is shown in Fig. 3d.

Scanning electron microscope (SEM) images further reveal the key free-standing microstructures in the fabrication process. Figure 4 shows the SEM image of MEMS switch with double-clamped membrane beam. Figure 4a demonstrates overall structure diagram of RF MEMS switch. Figure 4b, c detail magnified image of the free-standing membrane on the anchor air cavity, which is designed to prove sufficient support for the suspending membrane beam to ensure the successful fabrication. Moreover, the thin-walled anchor can be compatible with the thin metal deposition by magnetron sputter process. Figure 4d shows the membrane beam on the signal transmission line and the air gap between them. SEM results show that the key suspending parts of RF MEMS switch are clearly presented. Only through appropriate sacrificial layer preparation and release process and
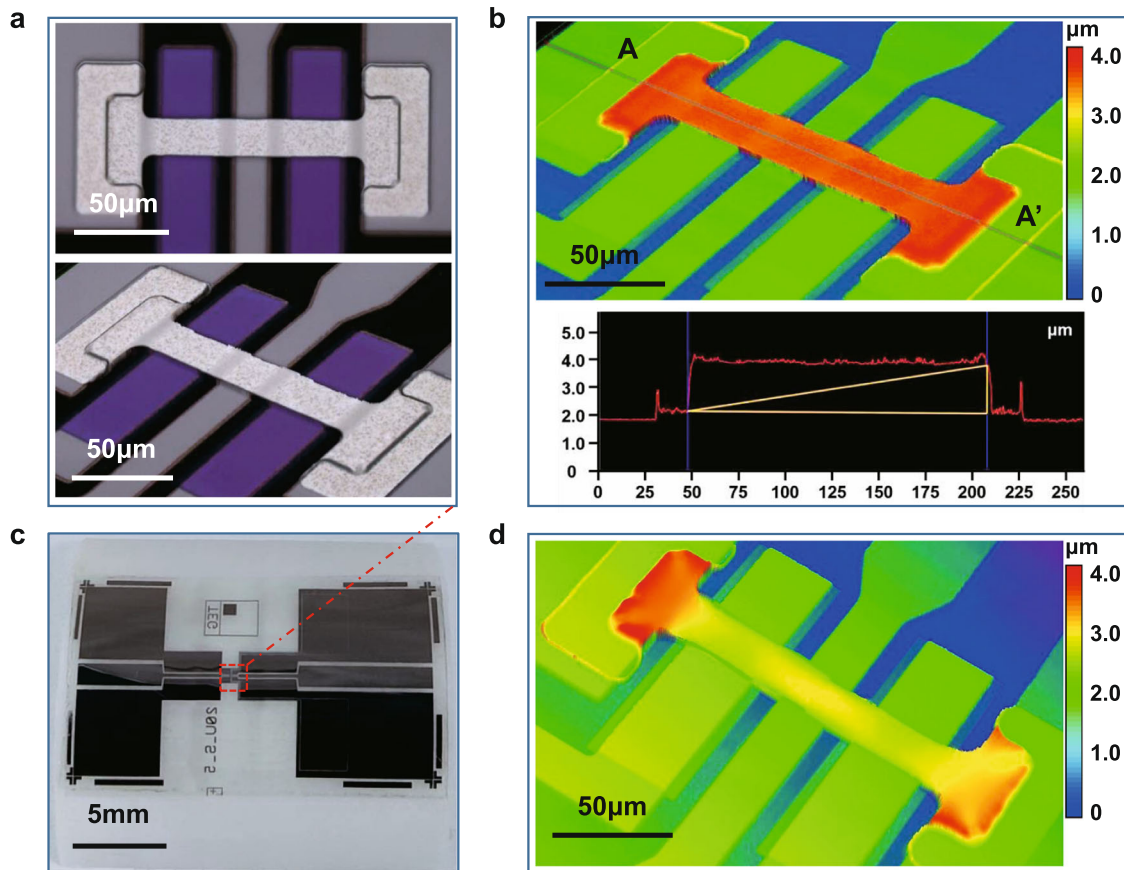
Fig. 3 Illustrations of fabricated flexible RF MEMS switch for characterization. a Optical microscope top view and oblique view of flexible RF MEMS switch. **b** Oblique view of 3D surface topography contour of flexible RF MEMS switch membrane beam. **c** Photograph of the flexible RF MEMS switch device bent on a curved surface. **d** Oblique view of 3D surface topography contour of flexible RF MEMS switch in membrane beam driving state. (Membrane beam width: 20 μm).

membrane beam metal layer deposition process can the suspending components with complete morphology be obtained (seen in Methods section for details).

Performance demonstration under bending deformation

The flexibility and RF characteristics of the flexible RF MEMS switch include the electrostatic driving and RF performance under different bending conditions, including the curvature of $0 \, \text{mm}^{-1}$ (flat substrate), $0.05 \, \text{mm}^{-1}$, and $0.1 \, \text{mm}^{-1}$. The instruments needed are as follows: vector network analyzer, DC voltage source, high-sensitivity digital multimeter, customized SMA connector and curved surface frames. The specific measurement physical diagram and the circuit diagram of the measurement platform are shown in Fig. 5a and Supplementary Fig. 7, respectively. The physics image and the structural design diagram of the customized SMA connector (RPC 2.92, R02K246-40ME3, Rosenberger) are shown in Fig. 5b and Supplementary Fig. 8. The FEA simulation process of flexible RF MEMS switch driven by electrostatic force under different bending condition is shown in Supplementary Fig. 9 and Supplementary Fig. 10. Based on the geometry obtained from electrostatic drive simulation, the RF characteristics simulation of switches with different configurations can be carried out. The results of experimental measurement and simulation analysis show that the driving voltage of flexible RF MEMS switch fabricated is 60 V under the bending curvature of $0 \, \text{mm}^{-1}$ (flat state) to $0.05 \, \text{mm}^{-1}$ and $0.10 \, \text{mm}^{-1}$.

Figure 6 demonstrates the S_{11} and S_{21} characteristics of the flexible RF MEMS switch under different bending condition measured by the measurement platform, together with the

corresponding simulation results. When the bending curvature varies from the $0 \, \text{mm}^{-1}$ (flat state) to $0.05 \, \text{mm}^{-1}$ and $0.10 \, \text{mm}^{-1}$, the return loss S_{11} of On state flexible RF MEMS switch is almost the same, which is less than $-18 \, \text{dB}$ in the frequency range of 17–19 GHz. The peak value of S_{11} within this frequency range changes from -23.0 dB to -22.3 dB, only decreasing by 3.0% (corresponding bending radius: 10 mm). The stability of RF performance under bending conditions is significantly better than the achievements listed in Table 1. Only the central frequency has a slight shifting, considering the impact of bending deformation on the CPW test port. The reason for the poor performance of S_{11} beyond the frequency range of 17–19 GHz is that the center frequency of the MEMS switch and the design frequency of impedance transformation are 17.7 GHz. Therefore, the RF characteristics that deviate from this frequency will introduce additional losses due to impedance mismatch. The RF performance beyond the frequency range of 17–19 GHz is random, with some frequency points having good performance and others having poor performance, shown in Supplementary Fig. 11. S_{11} of on state flexible RF MEMS switch shows the same tendency with S_{11}, which maintains in the range of $-4 \, \text{dB}$ to $-6 \, \text{dB}$ (S_{21} is relatively high, which is introduced by the DC drive electrode pads design in the CPW layer. See Supplementary Fig. 12 for details). The reason why the RF characteristics of on state flexible RF MEMS switch remain stable under different bending conditions is that the beam length (100 μm) is relatively small compared with the bending radius (10 mm or 20 mm). In this case, the suspending beam gap changes little, and the parallel capacitance of on state does not change significantly, so the impact on the RF
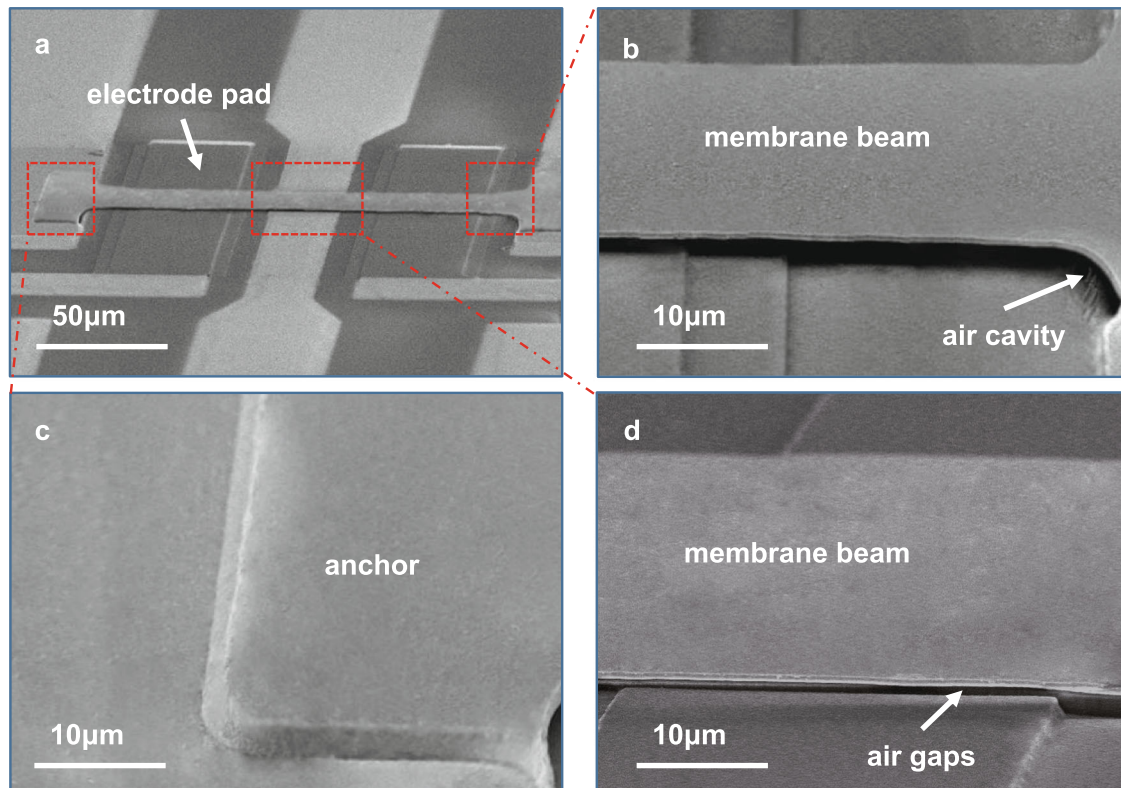
Fig. 4 SEM image of MEMS switch with double-clamped membrane beam. a Overall structure diagram of MEMS switch, (**b**) magnified image showing the free-standing membrane on air cavity at the anchor, (**c**) magnified image showing the anchor structure and (**d**) magnified image showing the membrane beam on the signal transmission line and the air gap between them.

characteristics can be almost ignored. For S_{11} and S_{21} of the off state, it can be seen from the results in Fig. 6e–h that there is almost no change in the off state S_{11} and S_{21} under different bending curvature. As already discussed, substrate bending has little effect on the RF performance of the switch in the driving state with the membrane beam. The relatively large difference occurs between and experiments for some results in Fig. 6, which is mainly caused by the deviation of the device fabrication process and the error in the measurement process. The characteristic impedances of the fabricated CPW measurement port, 1/4 λ impedance transformation and MEMS switch unit are not same as the designed value precisely. The factors that may cause performance deviation in the measurement process include impedance matching at the DC block and connectors in the measurement link.

Discussion on the applicable curvature of flexible RF MEMS switch

In order to systematically investigate the influence of bending curvature on the RF characteristics of flexible RF MEMS switch and find out the curvature range that can keep the RF characteristics of flexible RF MEMS switch stable, analysis of bending curvature influence on beam gap and RF characteristics is carried out, detailed analysis process shown in the Supplementary Note 2, Supplementary Figs. 13 and 14. And also, systematic parametric FEM simulations of the relationship between the flexible bending curvature and the RF characteristics of RF MEMS switch are performed.

Figure 7a shows the on state S_{11} variation with the substrate curvatures at 17–19 GHz. When the bending curvature is less than 0.2 mm^{-1}, S_{11} changes slightly from −26.7 dB to −24.5 dB. When the curvature increases from 0.2 mm^{-1} to 1 mm^{-1}, S_{11} changes

rapidly from −24.5 dB to −19.7 dB, which indicates that the bending curvature has a significant impact on the RF characteristics of the flexible RF MEMS switch. When the curvature continues to increase from 1 mm^{-1}, S_{11} sharply decreases from −19.7 dB to −0.28 dB when the curvature is 1.25 mm^{-1}. In this case, the bending deformation of the substrate has made the flexible RF MEMS switch unable to work normally. As the bending curvature continues to increase, S_{11} remains at about −0.1 dB, which is equivalent to the S_{11} value of the off state switch. This "off" state is due to the flexible bending deformation of the substrate. Figure 7b shows the on state S_{21} variation with the bending curvature at 17-19 GHz. When the bending curvature is less than 1.11 mm^{-1}, S_{21} changes slightly from −0.044 dB to −0.18 dB. This indicates that the effect of bending deformation on the RF characteristics of flexible RF MEMS switch can be almost ignored within this curvature range. However, as the curvature increases to 1.25 mm^{-1} or even to 2 mm^{-1}, S_{21} changes sharply to −31.1 dB and further to 41.8 dB, which is equivalent to the S_{21} value of the off state switch. The variation of on state S_{11} and S_{21} with the bending curvature is basically consistent with the variation of suspending beam with the bending curvature, which is obtained in Supplementary Note 2, Supplementary Figs. 13 and 14.

Figure 7c and d demonstrates the Off state S_{11} and S_{21} variation with the bending curvature at 17–19 GHz. It can be seen that S_{11} various from −0.075 dB to −0.1 dB and S_{21} various from -41.5 dB to -42.5 dB with the bending curvature increases to 2 mm^{-1}, corresponding to the curvature radius of 0.5 mm, which is already a considerable degree of bending deformation. These two parameters exhibit approximately horizontal with the change of curvature, indicating that S_{11} and S_{21} of the off state flexible RF MEMS switch are not affected by bending deformation. The reason for the above results is that the electrostatic driven
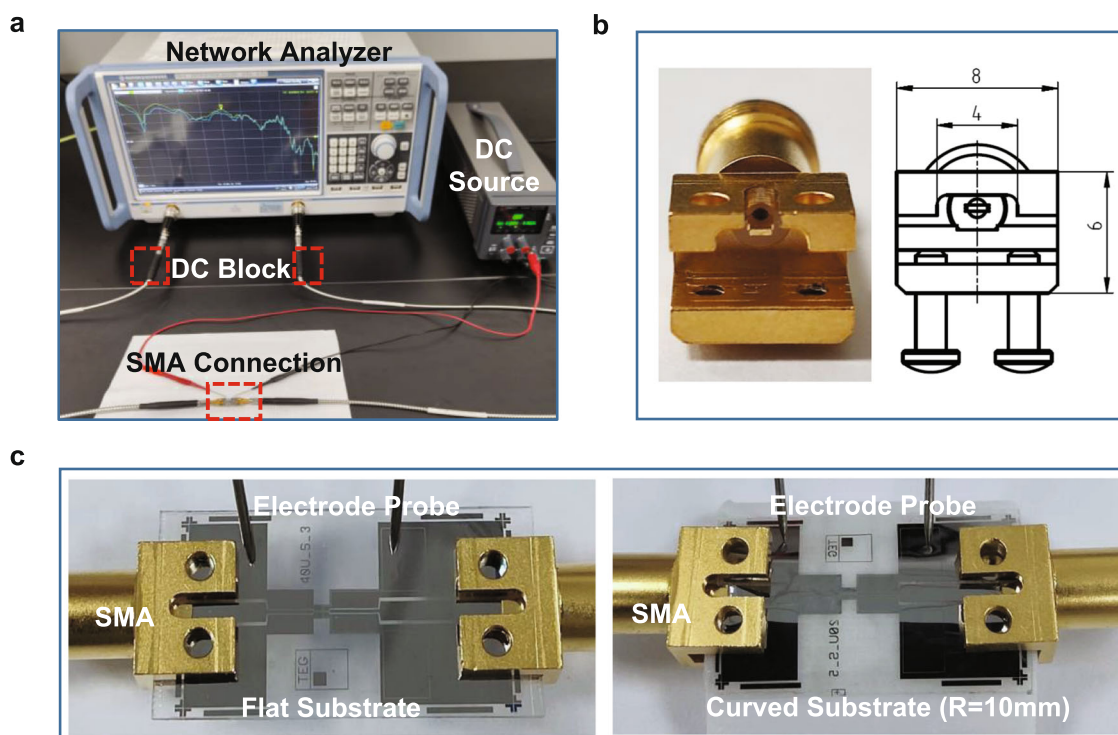
Fig. 5 RF performance measurement platform and SMA connector. a Measurement platform with network analyzer, DC source, DC block, SMA connection and probes. **b** The SMA connector used to measure the RF performance of the switch (Impedance: 50 Ω; Frequency: DC − 40 GHz). Connection diagram between (**c**) flat substrate and SMA, curved substrate (Radius: 10 mm) and SMA.

membrane beam is in contact with the signal line. Bending deformation will not transform the attachment state, which means no matter how large the bending curvature is, it will not have a significant impact on RF characteristics.

The RF performance of the fabricated flexible RF MEMS switch with measurement ports under larger bending curvature is as shown in Supplementary Fig. 15, which exhibits a consistent trend with the simulated results in Fig. 7. After exceeding the specific curvature (0.50 mm^{-1} for this device), the RF performance of the device deteriorates significantly with the increase of curvature for the On state MEMS switch.

DISCUSSION

In this work, we proposed a flexible RF MEMS switch, which is designed within the frequency band of 17–19 GHz towards satellite communication applications. The reflection loss (S_{11}) of the flexible RF MEMS switch at on state is exceeds -18 dB, with a driving voltage of 60 V, and maintains stable under the bending curvature of 0 mm^{-1}, 0.05 mm^{-1}, 0.10 mm^{-1}. S_{21} at on state meets the same tendency with S_{11}. Through systematic experimental measurement and simulation analysis, it is found that flexible RF MEMS switch can achieve certain bending radius by miniaturizing the electronic dimension, without degrading the RF performance. Furthermore, the range of bending curvature which will affect the RF characteristics is given through systematic simulation. The realization of flexible RF MEMS switch with high process compatibility and stable RF performance is a promising electronic component for future microwave communication and other applications of Flexible MEMS with movable components, with the advantages of light weight, high speed and low power consumption.

METHODS

Fabrication of the flexible RF MEMS switch

The fabrication process flow (Supplementary Fig. 5) is as follows: (i) Prepare 0.5 mm thick glass, clean it with acetone and ultrasonic, and then dry it in a 120 °C vacuum drying oven for 2 h. Use optically clear adhesive (OCA) glue to stick the 25 mm thick cop film material with 0.5 mm thick glass through a roller film applicator. (ii) To form the CPW layer patterned metal, metal layers (Mo/Al/Mo: 20 nm/1000 nm/20 nm) are deposited on COP film by sputter and then patterned through photolithography and wet chemical etching. (iii) Considering that the resistant temperature of flexible COP film material cannot exceed 130 °C, the low-temperature deposition process Thin Film Encapsulation Chemical Vapor Deposition (TFECVD, working temperature: around 85 °C) is used for dielectric layer (SiN$_x$: 1500 nm) deposition instead of Plasma-Enhanced Chemical Vapor Deposition (PECVD, working temperature: over 300 °C) in order to form the isolation layer on the driving electrode pads, and then patterned dielectric layer the through photolithography and patterned by reactive ion etching (RIE). (iv) Photoresist (AZ GXR 601) is used as the sacrificial layer material to prepare the sacrificial layer under the metal film beam. The thickness of the sacrificial layer should be controlled as required, which determines the gap between the metal membrane beam and the signal transmission line. It is worth noting that the photoresist forming the sacrificial layer should be naturally leveled for more than 30 minutes by standing horizontally in the fume hood before curing, so as to enhance the flatness of the sacrificial layer. (v) To form the patterned membrane beam, metal layers (Mo/Al/Mo: 10 nm/200 nm/10 nm) are deposited on the sacrificial layer by sputter and then patterned through photolithography and wet chemical etching. In order to reduce the residual stress of the membrane beam, the method of multiple deposition is used in the sputter deposition of the metal layer to prevent the temperature rise from being too high during the sputter process and to achieve the purpose of controlling the
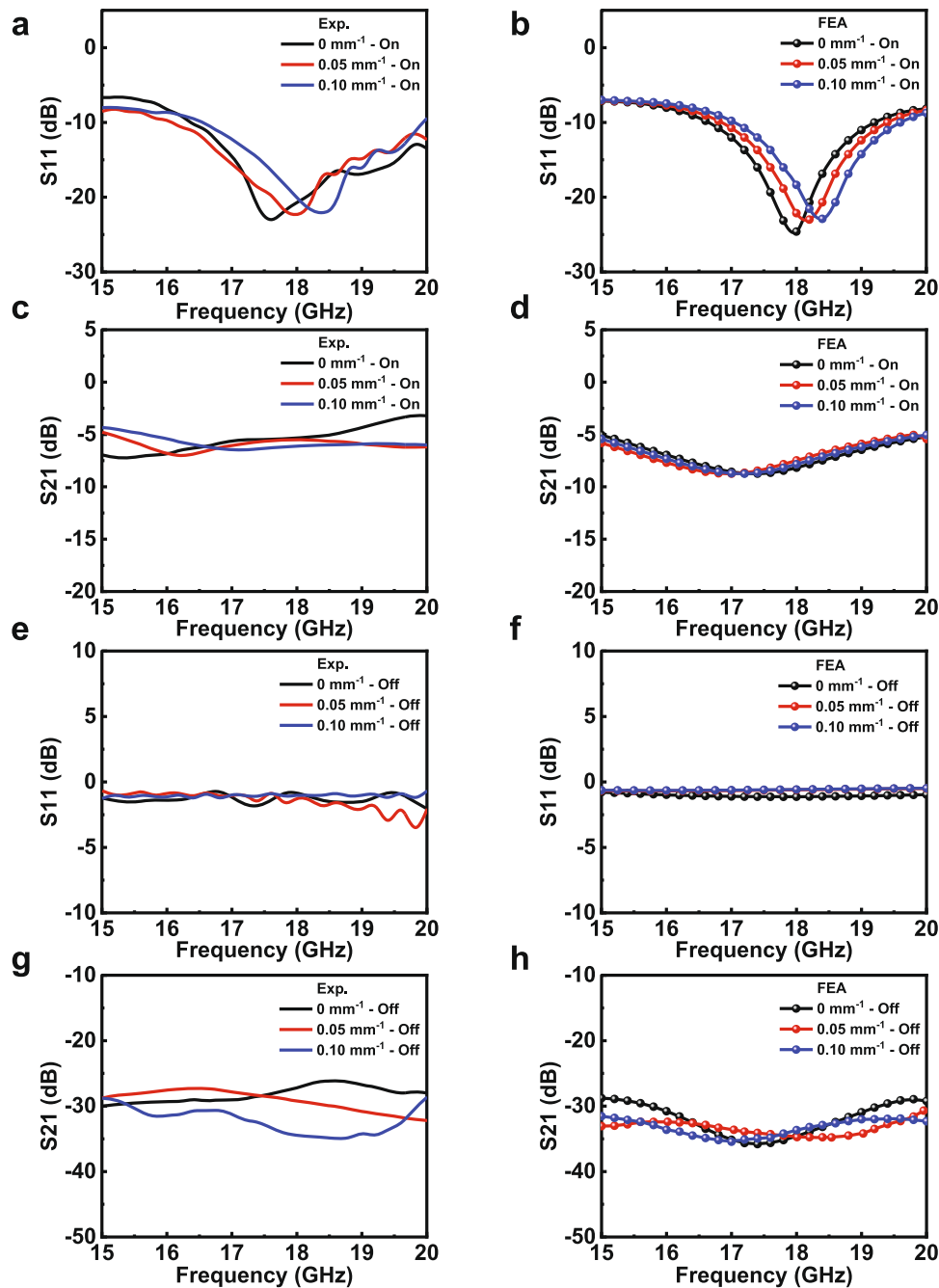
Fig. 6   RF characteristics under different bending curvatures. On state S_{11} of (**a**) experiment and (**b**) simulation; On state S_{21} of (**c**) experiment and (**d**) simulation; Off state S_{11} of (**e**) experiment and (**f**) simulation; Off state S_{21} of (**g**) experiment and (**h**) simulation under different bending curvatures radius of the flexible substrate.

residual stress of the membrane beam. (vi) The wet release technology is used to release the sacrificial layer. Put the sample with patterned membrane beam into degumming solution (AZ 300MIF) and maintain at 40 °C for 90 min. Then wash the sample with deionized water, put into deionized water and maintain for 10 min. Then put the sample into isopropyl alcohol (99.8%) and maintain for 300 min. Finally, place the sample in 60 °C vacuum drying oven for 60 min. (vii) Place the sample released from the sacrificial layer on the cold table for 2 min, and take advantage of the characteristic that the viscosity of OCA decreases with the temperature drop to realize the separation of the flexible COP film from the glass substrate, so as to peel off the flexible RF MEMS switch[57].

RF characteristics measurement of the flexible RF MEMS switch

The driving characteristics measurement platform (Supplementary Fig. 7) contains the following instrument: DC voltage source (KEYSIGHT, E36106B, DC Power Supply, 100 V, 0.4 A, 40 W), high-sensitivity digital multimeters (FLUKE, 150+ DIGITAL MULTIMETER), electrode probes and curved surface frames. Via this measurement platform, not only the driving characteristics of flexible RF MEMS can be measured, but also the structure of RF MEMS can be checked by observing the contact resistance through multimeter 2 under different driving states. The RF characteristics measurement platform (Fig. 5 and Supplementary Fig. 7) contains the following
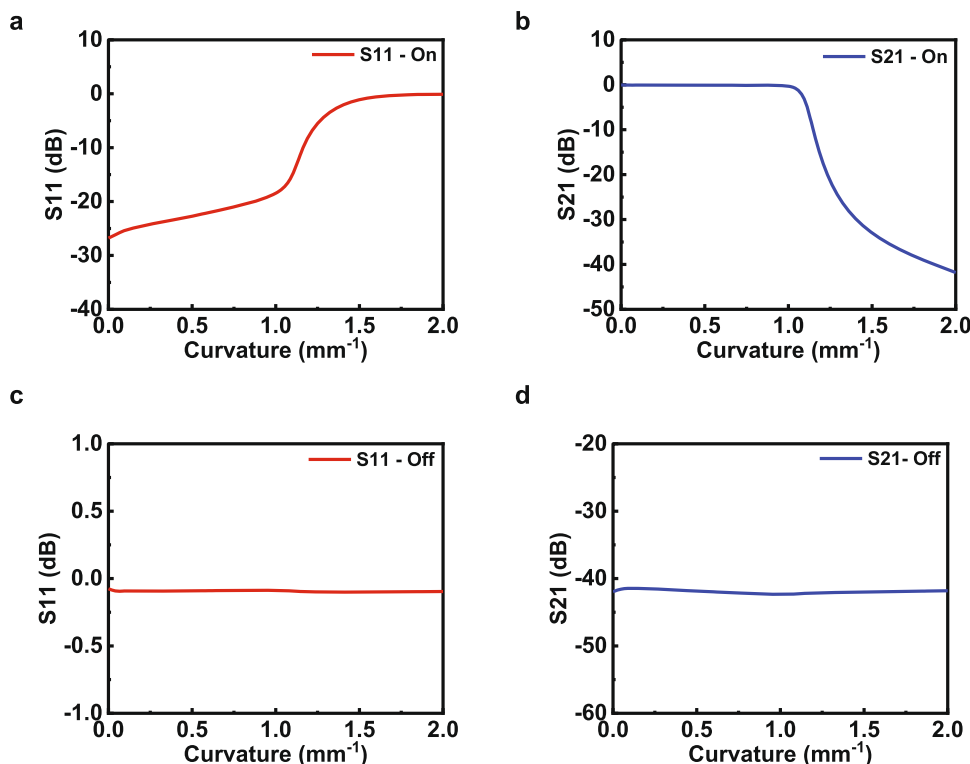
Fig. 7 Simulated RF characteristics of the RF MEMS switch with different bending curvatures. a On state S_{11}. **b** On state S_{21}. **c** Off state S_{11}. **d** Off state S_{21}.

instruments: vector network analyzer (ROHDE & SCHWARZ, ZNB-40, 10 MHz–40 GHz), DC voltage source (KEYSIGHT, E36106B, DC Power Supply, 100 V, 0.4 A, 40 W), DC Block, electrode probes and curved surface frames. Via this measurement platform, the RF characteristics of the switch in the on and off states under different bending curvatures can be realized.

FEM multi-physics field analysis

The multi-physical field simulation model is established in ANSYS workbench to investigate the flexible RF MEMS switch performance. Using the Static Structure module in the ANSYS Workbench, the topology transformation from flat flexible RF MEMS switch to flexible RF MEMS switch with different curvature is realized. Then, based on the geometric model before and after bending derived from the Static Structure module, the electrostatic field distribution of RF MEMS switch under different bias voltages is obtained by using the Maxwell 3D module in the ANSYS Workbench. Then, the electrostatic field distribution results are imported into the Static Structure module as the initial conditions. Under the initial conditions of the electrostatic load of the RF MEMS structure, the driving deformation simulation results of the RF MEMS membrane beam under the electrostatic force can be obtained. Till now, the RF MEMS switch geometric models under different curvature, before and after the membrane beam drive are obtained. By using the HFSS module integrated with the ANSYS Workbench, the RF characteristics of the RF MEMS switch under different states can be simulated. Considering the efficiency of modeling, the metal film beam layer of Mo/Al/Mo is replaced by a uniform Al metal layer. The thickness of CPW metal layer is 1 μm. The thickness of membrane beam if 200 nm. The thickness of COP substrate is 25 μm. The density, young's modules, Poisson's ratio, relative permittivity and bulk conductivity are 2770 kg m^{-3}, 7.1×10^{10} Pa, 0.33, 1 and 3.8×10^{10} Siemens m^{-1} for Al. The density, young's modules, Poisson's ratio, relative permittivity and dielectric loss tangent are 1700 kg m^{-3}, 2.47×10^{10} Pa, 0.17, 3.5, and 0.008 for COP.

REFERENCES

1. Araromi, O. A. et al. Ultra-sensitive and resilient compliant strain gauges for soft machines. *Nature* **587**, 219–224 (2020).
2. Ma, Y. J. et al. Flexible hybrid electronics for digital healthcare. *Adv. Mater.* **32**, 1902062 (2020).
3. Shi, X. et al. Large-area display textiles integrated with functional systems. *Nature* **591**, 240 (2021).
4. Zhang, Z. T. et al. High-brightness all-polymer stretchable LED with charge-trapping dilution. *Nature* **603**, 624 (2022).
5. Li, H. C. et al. Epidermal inorganic optoelectronics for blood oxygen measurement. *Adv. Healthc. Mater.* **6**, 9 (2017).
6. Shi, Y. et al. Functional soft composites as thermal protecting substrates for wearable electronics. *Adv. Funct. Mater.* **29**, 1905470 (2019).
7. Kim, B. H. et al. Three-dimensional electronic microfliers inspired by wind-dispersed seeds. *Nature* **597**, 503 (2021).
8. Liu, F. et al. Design and assembly of reconfigurable 3D radio-frequency antennas based on mechanically triggered switches. *Adv. Electron. Mater.* **5**, 1900256 (2019).
9. Fan, X. Q. et al. Mechanical terahertz modulation by skin-like ultrathin stretchable metasurface. *Small* **16**, 2002484 (2020).
10. Ozaki, T., Ohta, N., Jimbo, T. & Hamaguchi, K. A wireless radiofrequency-powered insect-scale flapping-wing aerial vehicle. *Nat. Electron.* **4**, 845 (2021).
11. Zeng, X. W. et al. A bioinspired three-dimensional integrated e-skin for multiple mechanical stimuli recognition. *Nano Energy* **92**, 106777 (2022).
12. Xiong, W. et al. Bio-inspired, intelligent flexible sensing skin for multifunctional flying perception. *Nano Energy* **90**, 106550 (2021).
13. Bai, H. D. et al. Stretchable distributed fiber-optic sensors. *Science* **370**, 848 (2020).
14. Wang, S., Luo, H., Linghu, C. & Song, J. Elastic energy storage enabled magnetically actuated, octopus-inspired smart adhesive. *Adv. Funct. Mater.* **31**, 2009217 (2020).

15. Liu, W., Song, M. S., Kong, B. & Cui, Y. Flexible and stretchable energy storage: recent advances and future perspectives. *Adv. Mater.* **29**, 34 (2017).

16. Huang, Z. et al. Three-dimensional integrated stretchable electronics. *Nat. Electron.* **1**, 473–480 (2018).

17. Song, H. L. et al. Highly-integrated, miniaturized, stretchable electronic systems based on stacked multilayer network materials. *Sci. Adv.* **8**, eabm3785 (2022).

18. Jiang, Y. et al. Flexible film bulk acoustic wave filters toward radiofrequency wireless communication. *Small* **14**, 1703644 (2018).

19. Sun, X. et al. Flexible lamb wave resonators with high figure of merit. *Appl. Phys. Lett.* **115**, 4 (2019).

20. Rai, T., Dantes, P., Bahreyni, B. & Kim, W. S. A stretchable RF antenna with silver nanowires. *IEEE Electron Device Lett.* **34**, 544–546 (2013).

21. Hussain, A. M. et al. Metal/polymer based stretchable antenna for constant frequency far-field communication in wearable electronics. *Adv. Funct. Mater.* **25**, 6565–6575 (2015).

22. Jung, Y. H. et al. Stretchable twisted-pair transmission lines for microwave frequency wearable electronics. *Adv. Funct. Mater.* **26**, 4635–4642 (2016).

23. Huang, X. et al. Highly flexible and conductive printed graphene for wireless wearable communications applications. *Sci. Rep.* **5**, 18298 (2015).

24. Patil, S. & Lee, D. W. Status review on the MEMS-based flexible supercapacitors. *J. Micromech. Microeng.* **29**, 093001 (2019).

25. Sun, L. et al. 12-GHz thin-film transistors on transferrable silicon nanomembranes for high-performance flexible electronics. *Small* **6**, 2553–2557 (2010).

26. Qin, G. et al. RF characterization of gigahertz flexible silicon thin-film transistor on plastic substrates under bending conditions. *IEEE Electron Device Lett.* **34**, 262–264 (2013).

27. Chang, H.-Y. et al. Large-area monolayer MoS_2 for flexible low-power RF nanoelectronics in the GHz regime. *Adv. Mater.* **28**, 1818–1823 (2016).

28. Wang, X., Liu, Y., Cheng, H. & Ouyang, X. Surface wettability for skin-interfaced sensors and devices. *Adv. Func. Mater.* **32**, 2200260 (2022).

29. Yi, N. et al. Fabricating functional circuits on 3D freeform surfaces via intense pulsed light-induced zinc mass transfer. *Mater. Today* **50**, 24–34 (2021).

30. Zhang, W. Q., Zhang, L., Liao, Y. B. & Cheng, H. Y. Conformal manufacturing of soft deformable sensors on the curved surface. *Int. J. Extrem. Manuf.* **3**, 042001 (2021).

31. Zhang, C. et al. Human motion-driven self-powered stretchable sensing platform based on laser-induced graphene foams. *Appl. Phys. Rev.* **9**, 011413 (2022).

32. Zhang, S. H. et al. Standalone stretchable RF systems based on asymmetric 3D microstrip antennas with on-body wireless communication and energy harvesting. *Nano Energy* **96**, 107069 (2022).

33. Liu, F. et al. High performance, tunable electrically small antennas through mechanically guided 3D assembly. *Small* **15**, 1804055 (2019).

34. Zhu, J. et al. Strain-insensitive hierarchically structured stretchable microstrip antennas for robust wireless communication. *Nanomicro Lett.* **13**, 108 (2021).

35. Mafinejad, Y., Ansari, H. R. & Khosroabadi, S. Development and optimization of RF MEMS switch. *Microsyst. Technol.* **26**, 1253–1263 (2020).

36. Petroni, S. et al. Flexible piezoelectric cantilevers fabricated on polyimide substrate. *Microelectron. Eng.* **98**, 603–606 (2012).

37. Kingsley, N., Ponchak, G. E. & Papapolymerou, J. Reconfigurable RF MEMS phased array antenna integrated within a liquid crystal polymer (LCP) system-on-package. *IEEE Trans. Antennas Propag.* **56**, 108–118 (2008).

38. Daneshmand, M. & Mansour, R. R. RF MEMS satellite switch matrices. *IEEE Micro Mag.* **12**, 92–109 (2011).

39. Jaafar, H. et al. A comprehensive study on RF MEMS switch. *Microsyst. Technol.* **20**, 2109–2121 (2014).

40. Farinelli, P. et al. Development of different K-band MEMS phase shifter designs for satellite COTM terminals. *Int. J. Microw. Wirel. T.* **2**, 263–271 (2010).

41. Rebeiz, G. M., Patel, C. D., Han, S. K., Ko, C. & Ho, K. M. J. The Search for a Reliable MEMS Switch. *IEEE Micro Mag.* **14**, 57–67 (2013).

42. Christodoulou, C. G., Tawk, Y., Lane, S. A. & Erwin, S. R. Reconfigurable antennas for wireless and space applications. *P. IEEE* **100**, 2250–2261 (2012).

43. Sailaja, B. V. S. & Naik, K. K. Design and analysis of compact antenna with cascaded elliptical patch for reconfigurability using RF switches at satellite applications. *Eur. Phys. J.* **136**, 346 (2021).

44. Dae-Hyeong, K. et al. Materials and noncoplanar mesh designs for integrated circuits with linear elastic responses to extreme mechanical deformations. *Proc. Natl Acad. Sci. USA* **105**, 18675–18680 (2008).

45. Sheng, X. et al. Stretchable batteries with self-similar serpentine interconnects and integrated wireless recharging systems. *Nat. Commun.* **4**, 1543 (2013).

46. Wang, G., Thompson, D., Tentzeris, E. M. & Papapolymerou, J. Low cost RF MEMS switches using LCP substrate. *Proc. 34th Eur. Microw. Conf.* **1-3**, 1441–1444 (2004).

47. Zhang, Q. X. et al. Development of RF MEMS switch on flexible organic substrate with wafer transfer technology (WTT). *Proc. 56th Electro Comp. Technol. Conf.* **1**, 523–527 (2006).

48. Patil, S. B., Chu, V. & Conde, J. P. Performance of thin film silicon MEMS on flexible plastic substrates. *Sens. Actuat. A-Phys.* **144**, 201–206 (2008).

49. Pestana, T. G. et al. Fabrication and characterization of thin-film silicon resonators on 10 mu m-thick polyimide substrates. *J. Micromech. Microeng.* **30**, 045007 (2020).

50. Han, L. & Gao, X. F. Modeling of bending characteristics on micromachined RF MEMS switch based on LCP substrate. *IEEE Trans. Electron Devices* **63**, 3707–3712 (2016).

51. Han, L., Yu, Y., Qin, R. J., Zhang, Z. Q. & Su, S. Static modeling of bending characteristics on V-shaped beam actuator based on flexible substrate. *Ieee Trans. Electron Devices* **66**, 5295–5300 (2019).

52. Han, L. et al. Multi-physical models of bending characteristics on the double-clamped beam switch for flexible electronic devices application. *Sensors* **20**, 16 (2020).

53. Han, L., Wang, R. & Chen, L. J. Bending characteristics of radio frequency microelectromechanical system low-pass filter based on flexible substrate. *Electron. Lett.* **57**, 860–862 (2021).

54. Zhang, Q. X. et al. RF MEMS switch integrated on printed circuit board with metallic membrane first sequence and transferring. *IEEE Electron Device Lett.* **27**, 552–554 (2006).

55. Teberio, F. et al. High-performance compact diplexers for Ku/K-band satellite applications. *IEEE Trans. Microw. Theory Tech.* **65**, 3866–3876 (2017).

56. D'arco, A. et al. Fabrication and spectroscopic characterization of graphene transparent electrodes on flexible cyclo-olefin substrates for terahertz electro-optic applications. *Nanotechnology* **31**, 364006 (2020).

57. Zhang, Y. X. et al. Mechanical behavior and constitutive model characterization of optically clear adhesive in flexible devices. *Micromachines* **13**, 301 (2022).

ACKNOWLEDGEMENTS

AUTHOR CONTRIBUTIONS
Y.S. and C.Z. designed the structure of the flexible RF MEMS switch. Y.S., Z.C., and Y.H. prepared the electronic devices. Y.S., J.G., C.L., and Q.W. characterized the performance. Y.S. did the simulation tests. Y.S. drafted the manuscript. Y.L. and Y.S. revised the manuscript. K.L. and Y.L. supervised the project. All authors read and approved the final manuscript.

COMPETING INTERESTS
The authors declare no competing interests.

ADDITIONAL INFORMATION
Supplementary information The online version contains supplementary material available at https://doi.org/10.1038/s41528-022-00214-3.

Correspondence and requests for materials should be addressed to Kui Liang, Yanzhao Li or Yuan Lin.

Reprints and permission information is available at http://www.nature.com/reprints

Publisher's note Springer Nature remains neutral with regard to jurisdictional claims in published maps and institutional affiliations.